Simulation of burr formation during single-pass honing of 4Cr13 stainless steel

Jiuhua Xu*, Shaowu Gao, Changyong Yang

College of Mechanical and Electrical Engineering, Nanjing University of Aeronautics and Astronautics, Nanjing, 210016, China

E-mail: jhxu@nuaa.edu.cn

Keywords: Sectional area, cutting depth, cutting width, inclination angle.

Abstract. Burrs inevitably appear in single-pass honing (SH) of ductile materials. As deburring is a non-productive operation, it should be eliminated or minimized to the greatest extent. And the principle of burr formation is the basis of burr active control. In this paper, a 3-D simulation model of single-grit micro-cutting was built by abstracting SH process. Simulations under different cutting parameters were carried out. And sectional area was used to evaluate the burr size. The simulated results showed that the burr size is mainly determined by the cutting state of hole edge. Reducing cutting width and cutting depth can efficiently diminish the size of burrs. Under the same material removal, warping burrs tend to form under small cutting parameters while crimped burrs tend to form under large cutting parameters. Inclination angle, which is the angle between cutting speed and rake face, has great influence on burr size. Increasing the inclination angle from -20° to 0°, the burr size increases rapidly from 9.126μm^2 to 22.38μm^2.

Introduction

Single-pass honing is widely used in manufacturing of precise holes with tight tolerance and good shape accuracy, such as valves. Burrs occur inevitably in most mechanical manufacturing process of ductile materials, including single-pass honing. And burrs have significant influence on the stability and reliability of honed parts [1]. Deburring is a non-productive operation and, as such, should be eliminated or minimized to the greatest extent possible [2].

The study on burr formation mechanism is the prerequisite for burr active control and burr minimization. In recent decades, many researchers have conducted both simulations and experiments on burr formation during tuning, milling and drilling process [3-10]. Some strategies to minimize the burrs have also been promoted based on the simulated and experimental results.

Due to large number of random cutting edges existing in grinding, shape of burrs formed in grinding is quite different with the ones in cutting. From the location, burrs in surface grinding can be divided into entrance burrs, exit burrs and side burrs [11,12]. As the growing direction of side burrs is vertical to the direction of cutting speed, in single-pass honing, the burrs in entrance and exit of holes can also be classified as side burrs in surface grinding.

For side burrs in surface grinding, several experimental researches have been carried out and the influence of grinding parameters on side burr size has also been clarified [11-13]. However, the experiments were conducted under large grinding depth, usually larger than 0.1mm. In single-pass honing, the cutting depth are generally smaller than 0.01mm, and the cutting trajectory of single grit are continuous.

Compared with experimental research, simulation seems to be a more efficient and economy way to study the burr formation mechanism. Existing simulation works on burr formation mainly concerned on the entrance and exit burrs with 2-D simulation models [14,15]. However,

side burrs can only be simulated in 3-D models. Therefore, in this paper, a 3-D simulation model of single-grit micro-cutting was built. Simulations under different cutting parameters were carried out to figure out the influence of cutting parameters on burr size.

Set-up of the simulation model

The diagram of single-pass honing is shown in Fig. 1. Generally, the workpieces are floating clamped on the worktable. Honing tools rotates at speed of n to remove workpiece material. And the feed is achieved by axial motion of honing tools at speed of v_a.

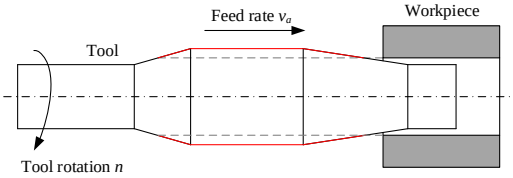

Fig. 1 Diagram of single-pass honing

The cutting trajectory of single grit in single-pass honing is helical. After unfolding the workpiece surface along the axis, the cutting trajectory turn to be straight, as shown in Fig. 2. And f and d are the feed per revolution and diameter of honing tools, respectively. In order to simplify the simulation models, only the local cutting states at the entrance and exit of workpiece were considered, as shown in Fig. 3.

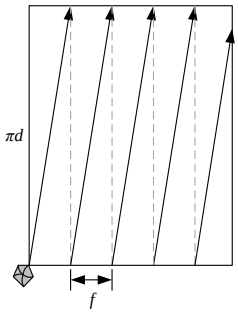

Fig. 2 Diagram of unfolded workiece surface

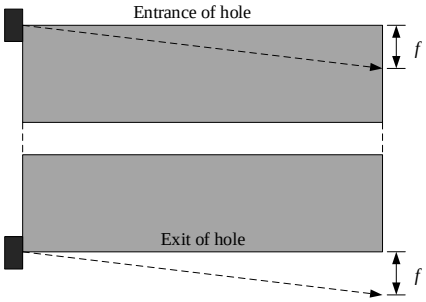

Fig. 3 Cutting states at the entrance and exit of holes

In this model, diamond was chosen as the tool material. The thermal conductivity is 138 W/m·K, heat capacity is 420 J/kg·K, and density is 3.5×10^3 kg/m^3. The geography parameters of single grit used in the model are shown in Fig. 4. The front angle of grit was set as -30°. And the radius of the cutting edge was set as 1μm. During the simulation, the grit was seen as a rigid body. The number of meshes of the grit was set as 8000 to ensure the accuracy of the details of the cutting edge.

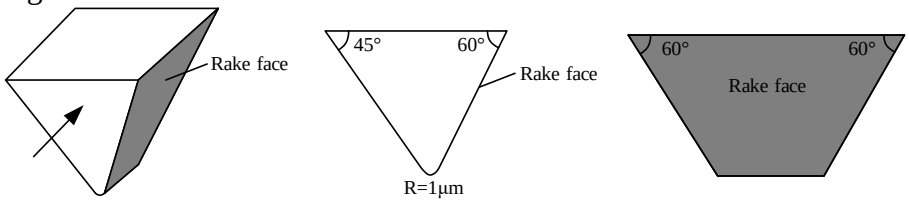

Fig. 4 Diagram of grian shape

1Cr13 martensitic stainless steel was used as workpiece material in the simulation model. The mechanical and physical properties of 1Cr13 are presented in Table 1. In order to model the plastic behavior of this material during the micro-cutting process, the Johnson–Cook material constitutive model is adopted. The J-C constitutive equation including five parameters can be described as follows:

$$\sigma = \left[A + B\varepsilon^n\right]\left[1 + C\ln\dot{\varepsilon}\right]\left[1 - \left(T^*\right)^m\right] \quad (1)$$

where A, B, and n are the three coefficients describing the quasi-static behavior of material, while C and m account for the strain rate hardening and thermal softening effects, respectively. $\dot{\varepsilon}$ is the reference strain rate. T^* is the homologous temperature and can be further defined by:

$$T^* = (T - T_r) / (T_m - T_r) \tag{2}$$

where T is the absolute temperature, T_r and T_m represent the room and melting absolute temperatures, respectively. And the parameters are shown in Table 2.

Table 1 The mechanical and physical properties of 1Cr13

Properties	Value
Density (kg/m^3)	7.75×10^3
Ultimate tensile strength (MPa)	711
Tensile yield strength (MPa)	583
Modulus of elasticity (GPa)	217
Thermal conductivity (W/m·K)	25
Poisson's ratio	0.28
Heat capacity (J/kg·K)	460

Table 2 The J-C equation parameters of 1Cr13

Parameters	A	B	C	T_m	T_r	n	m
Values	502	843	0.014	1500	20	0.148	0.509

The workpiece size was 100μm in length, 20μm in width and 15μm in height, as shown in Fig. 5. And the bottom face of the workpiece was fixed in the model. The workpiece was partitioned by tetrahedral meshes and the mesh number was 80000. Adaptive grid repartition method was adopted to avoid the mesh distortion. Shear friction was used to describe the friction state during simulation. The 3-D cutting model is shown in Fig. 6.

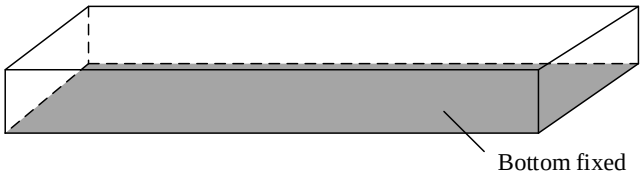

Fig. 5 Diagram of workpiece

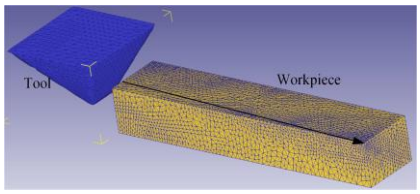

Fig.6 3-D cutting model

Simulations under different cutting depths, cutting widths cutting speeds and inclination angles are carried out. The cutting parameters are shown in Table 3. The workpiece after simulation was shown in Fig. 7(a). Side burrs produced during the cutting process were evaluated by the sectional area, as shown in Fig. 7(b).

Table 3 Cutting parameters of simulation

Parameters	Values
Cutting depth a_p (μm)	1, 3, 5
Cutting width a_e (μm)	1, 2, 3, 4, 5
Cutting speed v_s (m/s)	0.1
Inclination angle θ (°)	±60, ±50, ±40, ±30, ±20, ±10, 0

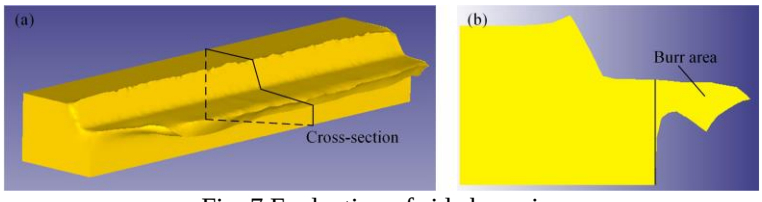

Fig. 7 Evaluation of side burr size

Results and discussion

Burr sectional areas at entrance and exit under v_s=0.1m/s, a_p=5μm, a_e=5μm, θ=0, are shown in Fig. 8. It can be seen that, under the same cutting parameters, burrs at exit are larger than the ones at entrance. Compared with cutting at exit, when cutting at entrance, the feeding direction is opposite to the burr growing direction, restraining the formation of side burrs to a certain extent.

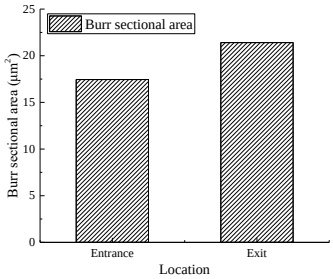

Fig. 8 Burr sectional areas at entrance and exit (v_s=0.1m/s, a_p=5μm, a_e=5μm, θ=0)

Fig. 9 shows the burr sectional areas under different cutting widths. It can be seen that the burr size increase rapidly from 10.02μm^2 to 29.29μm^2 with the increasing of cutting width from 1μm to 5μm. Side burrs during cutting come from both plastic deformation of workpiece caused by cutting force and plastic flow of cutting layer. Larger cutting widths accompany with more heavy cutting forces and larger cross-sectional areas of cutting layer, resulting in larger burrs.

When keeping cutting width at 1μm, accumulated cutting width increases. Burr sectional areas with different accumulated cutting widths are shown in Fig. 10. And the burr sectional topography are shown in Fig. 11(a) to Fig. 11(e). It can be concluded that the burrs are mainly caused by the material removal near the edge. Besides, by comparing Fig. 11(d) and Fig. 11(f), it can be seen that burrs can be diminished by using smaller cutting width while under the same material removal.

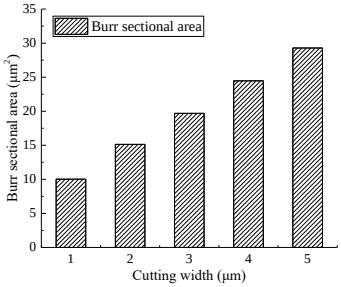

Fig. 9 Burr sectional areas under different cutting widths (v_s=0.1m/s, a_p=5μm, θ=0)

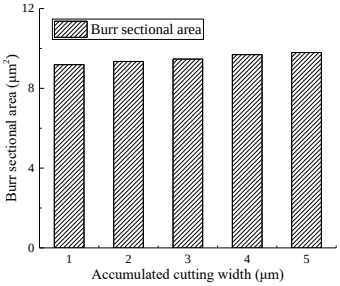

Fig. 10 Burr sectional areas vs. accumulated cutting widths (v_s=0.1m/s, a_p=5μm, a_e=1μm, θ=0)

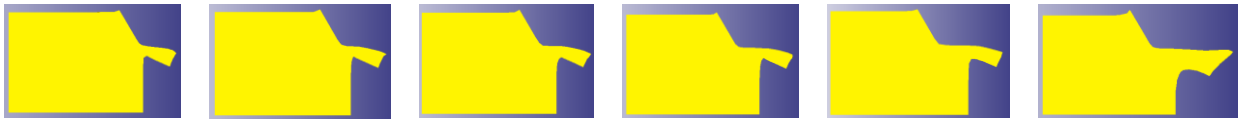

(a) a_e=1μm, P=1 (b) a_e=1μm, P=2 (c) a_e=1μm, P=3 (d) a_e=1μm, P=4 (e) a_e=1μm, P=5 (f) a_e=4μm

Fig. 11 Burr sectional topography under different cutting parameters (v_s=0.1m/s, a_p=5μm, θ=0)

Burr sectional areas under different cutting widths are shown in Fig. 12. It can be seen that burr size increses significantly with the increase of cutting depth as a reslut of the increase of

cutting force and cross-sectional areas of cutting layer. Fig. 13 shows the burr sectional area with different accumulated cutting depths. Burr sectional topography under different cutting depths are shown in Fig. 14. It can be concluded that, with the increase of accumulated cutting depth, burr size increase steadily. In addition, under the same material removal, simulation with smaller cutting depth can obtain smaller burrs. And burrs forming under small cutting depth tend to be narrow and crimped.

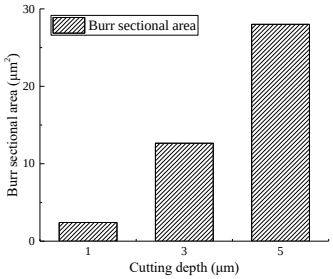

Fig. 12 Burr sectional areas under different cutting depths (v_s=0.1m/s, a_e=5μm, θ=0)

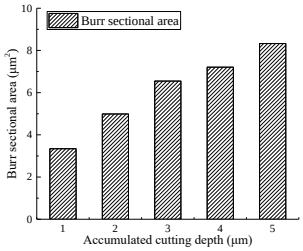

Fig. 13 Burr sectional areas vs. accumulated cutting depths (v_s=0.1m/s, a_e=5μm, a_p=1μm, θ=0)

(a) a_p=1μm, P=1 (b) a_p=1μm, P=2 (c) a_p=1μm, P=3 (d) a_p=1μm, P=4 (e) a_p=1μm, P=5 (f) a_p=5μm

Fig. 14 Burr sectional topography under different cutting parameters (v_s=0.1m/s, a_e=5μm, θ=0)

Fig. 15 shows the relative position between grains and workpiece under different inclination angles. The sectional areas of cutting layer were kept constant by adjusting the model of grains. The rake angle and radius of cutting edge were also remain constant. The burr sectional areas and topography under different inclination angles are shown in Fig. 16 and Fig. 17, respectively. It can be seen that the negative inclination angle can efficiently diminish the size of burrs at exit. The reason is that, different with positive inclination angle, negative inclination angle lead the workpiece material of cutting layer flowing inwards, rather than outwards, as shown in Fig. 17.

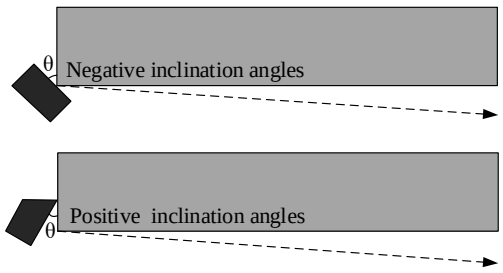

Fig. 15 Diagram of simulation model under different inclination angles

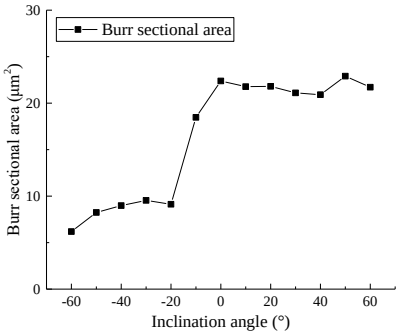

Fig. 16 Burr sectional areas under different inclination angles (v_s=0.1m/s, a_e=5μm, a_p=5μm)

(a) θ=-60° (b) θ=-20° (c) θ=-10° (d) θ=0 (e) θ=60°

Fig. 17 Burr sectional topography under different cutting parameters (v_s=0.1m/s, a_e=5μm, a_p=5μm)

Conclusions

Simulation works on side burrs fomation under different cutting parameters were conducted with a 3-D simulation model. The results showed that side burrs during cutting come from both plastic deformation of workpiece caused by cutting force and plastic flow of cutting layer. Under the same cutting parameters, burrs at exit are larger than the ones at entrance. Besides, reduction of cutting width and cutting depth can both diminish the size of burrs. Compared with positive inclination angle, cutting under negative inclination angle can efficiently decrease the size of side burrs, especially when inclination angle is smaller than -20°.

References

[1] D. Dornfeld, S. Min, A Review of Burr Formation in Machining, in: J Aurich., D Dornfeld. (Eds.), Burrs - Analysis, Control and Removal, Springer, Berlin, Heidelberg, 2010, pp. 3-11.

[2] J. C. Aurich, D. Dornfeld, P. J. Arrazola, V. Franke, L. Leitz and S. Min, Burrs— Analysis, control and removal, CIRP Ann. Manuf. Technol. 58(2009) 519-542.

[3] J. Lu, J. Chen, Q. Fang, B. Liu, Y. Liu and T. Jin, Finite element simulation for Ti-6Al-4V alloy deformation near the exit of orthogonal cutting, Int. J. Adv. Manuf. Technol. 85(2016) 2377-2388.

[4] W.J. Deng, W. Xia and Y. Tang, Finite element simulation for burr formation near the exit of orthogonal cutting, Int. J. Adv. Manuf. Technol. 43(2009) 1035-1045.

[5] L. K. L. Saunders, A finite element model of exit burrs for drilling of metals, Finite Elem. Anal. Des. 40 (2003) 139-158.

[6] K. Saptaji, S. Subbiah, J.S. Dhupia, Effect of side edge angle and effective rake angle on top burrs in micro-milling, Precis. Eng. 36 (2012) 444-450.

[7] R. Lekkala, V. Bajpai, R.K. Singh, S.S. Joshi, Characterization and modeling of burr formation in micro-end milling, Precis. Eng. 35 (2011) 625-637.

[8] T. Lin, Experimental study of burr formation and tool chipping in the face milling of stainless steel, J. Mater. Process Tech. 108 (2000) 12-20.

[9] L.K. Lauderbaugh, Analysis of the effects of process parameters on exit burrs in drilling using a combined simulation and experimental approach, J. Mater. Process Tech. 209 (2009) 1909-1919.

[10] Y.B. Guo, D.A. Dornfeld, Finite Element Modeling of Burr Formation Process in Drilling 304 Stainless Steel, J. Manuf. Sci. Eng. 122 (2000) 612-619.

[11] J.C. Aurich, H. Sudermann, H. Bil, Characterisation of Burr Formation in Grinding and Prospects for Modelling, CIRP Ann. Manuf. Technol. 54 (2005) 313-316.

[12] H. Sudermann, I.G. Reichenbach, J.C. Aurich, Analytical Modeling and Experimental Investigation of Burr Formation in Grinding, in: J Aurich., D Dornfeld. (Eds.), Burrs - Analysis, Control and Removal, Springer, Berlin, Heidelberg, 2010, pp. 63-71.

[13] J.C. Aurich, H. Sudermann, O. Braun, Experimental Investigation of Burr Formation in the Surface Grinding of Tool Steel, P. I. Mech. Eng. B-J. Eng. 220 (2006) 489-497.

[14] D. Fu, W. Ding, S. Yang, Q. Miao, Y. Fu, Formation mechanism and geometry characteristics of exit-direction burrs generated in surface grinding of Ti-6Al-4V titanium alloy, Int. J. Adv. Manuf. Technol. 89 (2017) 2299-2313.

[15] D. Dong, J. Song, D. Yu, M. Chen, Finite element analysis of burr formation and an automatic online micro-deburring method in precise end-face grinding process, P. I. Mech. Eng. B-J. Eng. 231 (2017) 2495-2503.